Re-entry Prediction Uncertainties derived from Environmental and Observation considerations

Noelia Sánchez-Ortiz[(1)], Nuria Guijarro López[(1)], Ignacio Grande[(1)], Luis Tabera[(1)], Adam White[(1)], Sean Bruinsma[(2)], Stijn Lemmens[(3)]

[(1)] Deimos Space, Ronda de Poniente 19, 28760, Tres Cantos, Madrid, 28760, Spain,
Email: noelia.sanchez@deimos-space.com

[(2)] CNES, Toulouse, France
Email: sean.bruinsma@cnes.fr

[(3)] ESA/ESOC Space Debris Office (OPS-GR), Robert-Bosch-Str. 5, 64293 Darmstadt, Germany,
Email: stijn.lemmens@esa.int

ABSTRACT

The GOCE re-entry, occurred in October/November 2013, provided an outstanding data set for analysing the re-entry of this objects, and derive lessons learnt for re-entry predictions of other space objects.

Among other aspects, the GOCE re-entry data allows evaluating the impact of the variation of the various physical and environmental parameters to the estimated re-entry time, assessing how they affect the re-entry estimations, and to investigate the optimal observation planning to minimise the uncertainties on the re-entry predictions.

In regards to environmental aspects, the paper describes the impact of the atmosphere uncertainties derived from a lack of knowledge of space weather aspects. The impact of solar activity in re-entry prediction and the forecast uncertainty is analysed to assess the capability to accurate predict re-entries. The impact of unexpected solar storms is also described.

Regarding the observational aspects, the paper describes the achievable accuracy on the estimation of the position and velocity of a re-entering object, and how it is translated into the re-entry prediction errors, through montecarlo analysis. Different sensor architectures and observation approaches are analysed in order to determine the most suitable observation approach for those kind of events, accounting for one or more radar stations.

This paper summarises the work done within the ESA PREGO activity (4000115173/15/F/MOS) by Elecnor DEIMOS, in collaboration with CNES and AIUB.

1 INTRODUCTION

The objective of ESA PREGO activity (ESA/ESOC contract 4000115173/15/F/MOS) is to improve the capacities on re-entry prediction thanks to a complete analysis of the outstanding data set related to the GOCE re-entry occurred in October/November 2013.

From the available GOCE data set composed of: GOCE level 1b dataset for orbit and attitude precise determination (GPS and Quaternion data) and special data set; TIRA radar observations (range, range-rate, azimuth, and elevation measurements), GOCE satellite 3D model and thermodynamic features and GOCE TLE data along the re-entry phase, three interrelated tasks are undertaken.

First task regards to high accuracy orbit determination of the GOCE orbit along the re-entry period. Reduced-dynamic and kinematic orbit estimation has been applied for this task. In order to ensure this accuracy, several Precise Orbit Determination techniques were applied in order to select the most appropriate one. As the atmospheric density is one of the main aspects playing a role in the capability of determining the re-entry time and location, it has been accurately modelled the effects of the environmental aspects, by evaluation of the main thermosphere models and their input parameters.

Once the reference data is available, in particular the accurate re-entry orbit, the derived information from the first task has been used for a dynamic and observational model analysis focusing on the GOCE object. This paper describes the two type analysis done in this regard and provide some conclusions on them.

A final task has also been executed in order to exploit the results and conclusions obtained from dynamic and

observational model analysis in terms of re-entry uncertainties models to space objects with aerodynamics characteristics similar to GOCE; i.e. elongated rigid bodies like rocket stages, platforms or payloads. More information can be obtained in [2].

2 DYNAMIC MODEL ANALYSIS

The **dynamic model analysis** intends to provide a re-entry time error budget allocation with respect to uncertainties on the most relevant parameters. This is done by a sensitivity analysis that takes into account all the inter-relationships between the different variables playing a role in an objects orbit. The sensitive analysis focuses on the GOCE orbit. All variables are varied according to their expected and predicted behaviour.

Among the different parameters or issues considered, it has been evaluated the impact on re-entry date estimation of the uncertainty in orbital estimation, the drag coefficient and space weather considerations, among them, the occurrence of some special events, but also the effect of the lack of knowledge of space weather. A comparison between the estimated and observed solar activity is done, with analysis on the re-entry estimation capability.

The nominal case for analysis has been selected so that it covers the last 24.75 days before re-entry.

2.1 Orbital Uncertainty influence on the estimation of re-entry date

Several test cases have been run in order to evaluate the impact of orbit uncertainty, both in position and velocity, of the initial orbit in the re-entry epoch. The analysis is done by means of Monte Carlo simulations assuming that the initial state vector has an associated covariance matrix that determines its uncertainty. For each run of the Monte Carlo execution, a sample state vector is obtained by sampling the covariance matrix and propagated until it reaches an altitude of 80 km.

Cases varying the position and/or velocity uncertainty were first run, by considering spherical uncertainty over the state vector.

First, a simple 3 dimensional position-only covariance matrix in the inertial frame with 1 km sigma is used. A set of 10,000 runs are executed and the resulting histogram is shown in Figure 1. The plot shows a normal-like distribution with an average close to the nominal re-entry time of 24.75 days, together with some other fitting with well-known distributions, with its computed K-S score. Figures are provided in absolute and relative values with respect to the total estimated time to re-entry.

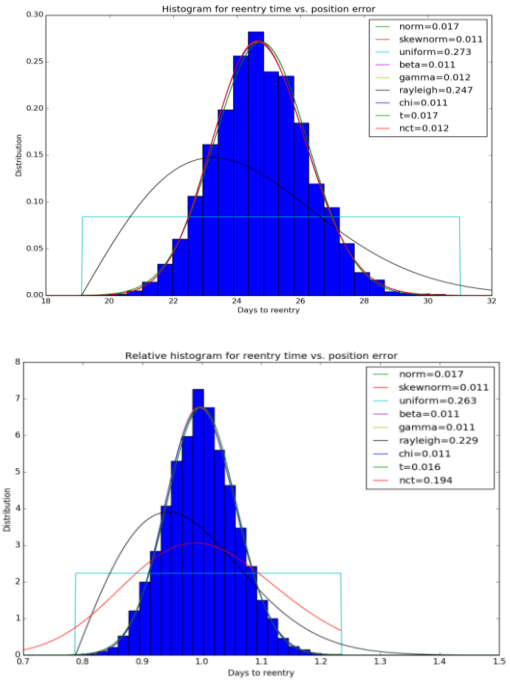

Figure 1: Histograms for re-entry time vs. position error with fitting (bottom, relative distribution)

Skewed normal distribution tends to fit well with the results from the simulated cases. Mean and standard deviation for the skewed normal is 24.75 days and 1.47 days respectively.

By analysing the orbital uncertainties derived from processing radar observations (next section of the paper), it can be seen that a rough 0.1 km and 1 m/s position and velocity error can be assumed, if considering a spherical error. Thus, this particular case has also been analysed before assessing the impact of not spherical covariance. Results are shown in this figure, with deviations of about 30% in the re-entry prediction times.

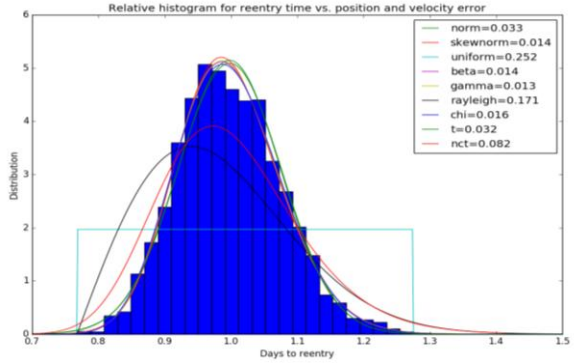

Figure 2: Relative histogram for re-entry time vs. position and velocity error with fitting, for the case of spherical covariance errors of 0.1km and 1 m/s

Position and velocity errors are normally not spherical. So the Along-track, Cross-track and Radial typical computed from the observational analysis have been used to feed a non-spherical covariance and assess the impact in the re-entry prediction capability. In addition to these nominal non-spherical covariance ellipsoids, two additional cases have been analysed in order to determine the impact of having a one-order of magnitude better and worse uncertainty. The projected ellipsoids in the XY and Vx Vy plane are shown in Figure 3.

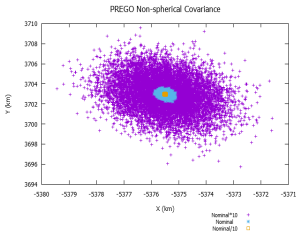

Figure 3: Initial position and velocity covariance, three cases analysed

When considering the nominal non-spherical covariance, the re-entry prediction time deviates about ±15% from the nominal prediction.

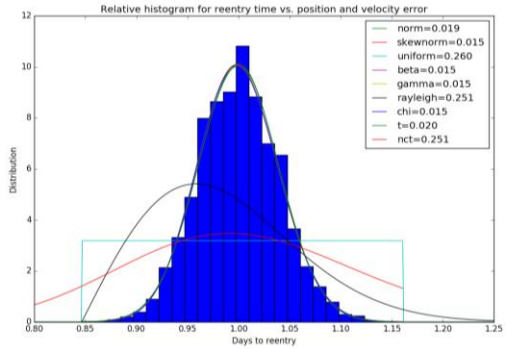

Figure 4: Relative histogram for re-entry time vs. position and velocity error with fitting, for the case of nominal non-spherical position and velocity uncertainties

In case the uncertainty is ten times that obtained for the nominal case (processing the radar observations), we can see in next figure (upper plot) that the re-entry prediction has a strong variability, reaching prediction times which are well over 100% prediction times over the nominal case. This is caused by the large uncertainty imposed in the velocity estimation. In the case the nominal uncertainty (as from the case above) is imposed for the velocity and the position is considered ten times worse than the nominal case, the predictions are constrained in about a ±30% time prediction error. In this particular case, and due to the larger prediction times associated to slightly higher points within the position covariance ellipsoid, a slightly displaced distribution is observed.

Similarly, a case for a position and velocity uncertainty ten times smaller than the nominal one has been analysed. In this particular case, the deviations are so small that it is almost not observable when plotting the obtained distribution from the Monte Carlo analysis.

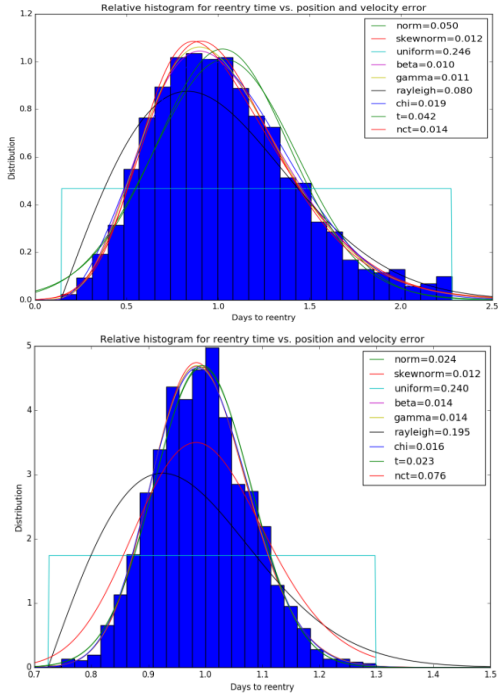

Figure 5: Relative histogram for re-entry time vs. position and velocity error with fitting, for the case of non-spherical position and velocity uncertainties ten times larger than the nominal one (upper plot) and considering ten times factor for position and nominal velocity covariance (right plot)

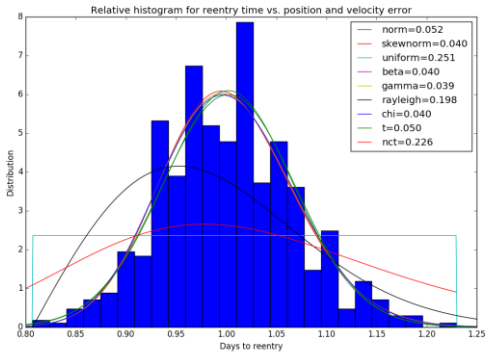

Figure 6: Relative histogram for a re-entry time of 5 days vs. position and velocity error with fitting, for the case of spherical covariance errors of 0.1km and 1 m/s.

The impact of orbital uncertainty for different times to re-entry was also analysed, by repeating the simulation case with errors in position and velocity of 0.1 km and 1 m/s respectively, Monte Carlo simulation has been executed moving the orbit until a time for re-entry around 20 days (nominal case reported above lasts for 24.7 days). Subsequently, the same procedure will be done with 15, 10 and 5 days. Only the result for the case of 5 days to re-entry is shown in Figure 7.

Results for the different prediction times analysed so far, are summarised in the following graph. As it can be seen, large relative re-entry deviations are obtained during the latest days before actual re-entry (analysed case, 5 days before re-entry), which seems to be derived from the larger influence of the drag perturbation when considering slightly different initial position and velocity state vectors. Former to this very latest moments, the relative deviation diminishes.

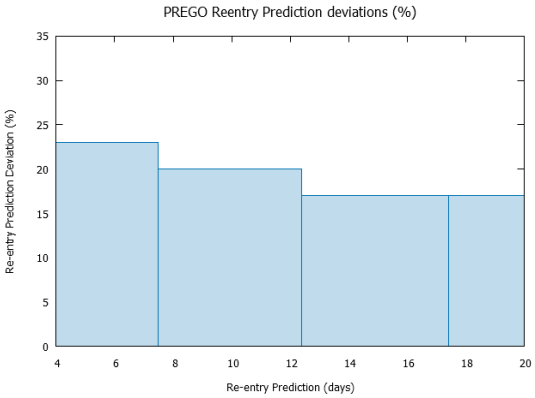

Figure 7: Relative Re-entry time deviations as a function of the re-entry time prediction.

2.2 Impact of General Space Weather Conditions

In order to analyse the space weather conditions on re-entry time, real observed data have been used, from the 55 years of archive data. For each day in the space weather records, a time shift is applied, replicating past space weather conditions to the day of the reference orbit. Then the orbit is propagated as usual until the re-entry altitude of 80 km.

Next figure provides the time to re-entry if the initial conditions are set at different dates along the 55 years. For example, if the Re-entry propagation is initiated in January 1960, the re-entry lasts for about 17 days, whereas in case the initial conditions are set in January 2010, the re-entry period is about 35 days. Such variability is due to the solar activity conditions, which have a strong impact on atmospheric density and hence the re-entry propagation.

Interestingly, the plot is approximately an inverted graph of the solar cycle activity, as expected. Higher solar activity means a denser upper atmosphere thus more drag and earlier re-entry time. The comparison between the re-entry time and the F10.7 average flux can be found in Figure 8, where valleys in solar activity directly translate to peaks in re-entry time, and vice-versa.

It can be observed that the minimum corresponding to the solar maximum at 2013 is higher than other points at such conditions activity. It seems to be related to the fact that the latest solar maximum period was indeed a period with lower activity than previous cycles. This can also be observed at the solar maximum activity period around 1970.

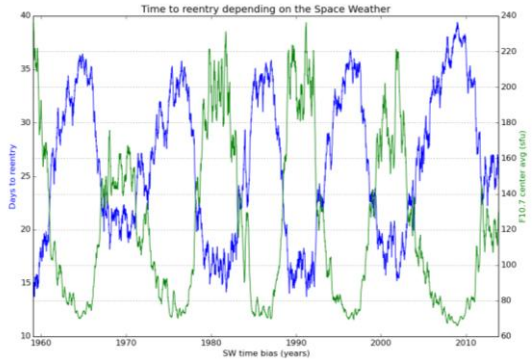

Figure 8: Re-entry time and F10.7 81-day average flux

This correlation between the re-entry time and the solar flux can be explored using a scatter plot of the two values. Such a plot can be seen in Figure 9. The plot shows an inverse correlation: the higher the flux, the shorter the re-entry time. This is expected by the inverse correlation shown in Figure 8, but it clearly shows that short re-entry times can also be present with low F10.7 flux (left of the image). This can be explained by the re-entry time of about 15-20 days for peaks of activity; the flux may present rapid variations in that period of time, having peaks that affect the re-entry time.

On the contrary, when the same comparison is done against the daily Ap value, the same correlation cannot be seen as clearly as before. There is some correlation, in particular in the valley of 2010, but not as clear as in the F10.7 case. Figure 10 shows the scatter plot between the re-entry time and the Ap index, and while some slight correlation can be seen, in particular, there is a trend where higher re-entry time has lower maximum Ap index, but it is not as clear as in the F10.7 case.

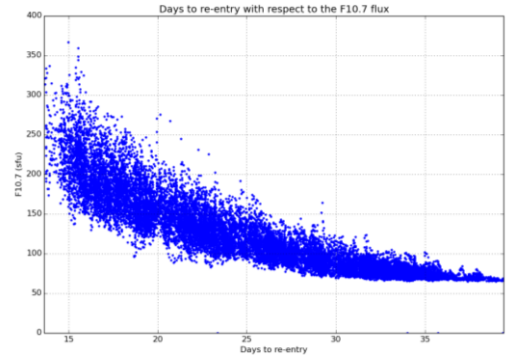

Figure 9: Days to re-entry wrt. the F10.7 flux

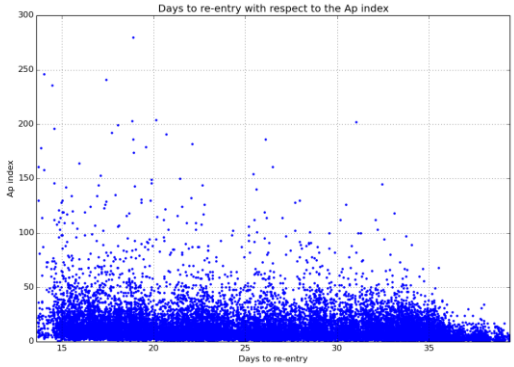

Figure 10: Days to re-entry wrt. the Ap index

The histogram for this data set is quite complex (difficult to derive conclusions), and no standard distribution tested matches very well the empirical distribution, as shown in Figure 11. In this case may be the uniform distribution could be used as an approximation.

The lower probability on both extremes means that extreme space weather conditions, both too active and too weak, are rare. The peak around 35 days corresponds to the long calm periods between active solar peaks.

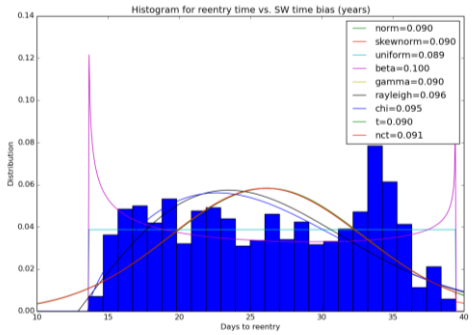

Figure 11: Histogram for re-entry time vs. previous space weather conditions

Figure 8 covers about 55 years of solar activity; however it is interesting to investigate the different phases of the solar cycle considering four regions. Histogram data for each region has been considered separately, but every region of the same kind is analysed together, that is, all high solar cycle regions are put together and the combined data is used to create the histogram. Results are summarised in the following:

- "high" solar cycle, where the F10.7 flux is at its peak. It usually is above 100-150 sfu. These regions correspond to the shortest re-entry epochs, due to the increased activity (mean re-entry time is about 19 days). In this case, a skewed normal gives a good fit, but there are some gaps and peaks out of the distribution. This is because only five peak regions are available. While each peak region is approximately of the same magnitude, there are differences of peak flux among cycles. For example, the 21 days peak in the middle of the histogram can be traced to the years 1968-1971, which had a lower flux and thus longer re-entry time than the other peak periods.
- "low" solar cycle, where the F10.7 flux is lower than 75 sfu. As expected, it corresponds to the longest re-entry times (the mean is around 35 days). A peak at 38 days has been found corresponding the unusually quiet and long minimum from 2005-2010.
- "up" and "down" are the regions between peaks and valleys where the flux goes up and down respectively.). In these cases, the re-entry times are distributed between the re-entry times of valleys and peaks of the solar activity. This distribution makes the normal or skewed normal distribution not as good as in the previous cases. The fittest tested distribution is beta, however, there is no reason to think that the re-entry times actually follow a beta distribution (the fit is not very good and there are some outliers), but that the general shape of the empirical distribution is simply closer to the beta probability distribution function.

Table 1 shows the mean, standard deviation and skewness for the skewed normal distributions resulting of fitting the entire 55-year period, and divided in solar cycle phase. "up" and "down" regions, having a worse fitting than the other regions, also present a higher standard deviation.

Table 1: Skewed normal fitted values for nominal space weather

Region	Mean (days)	Standard deviation (days)	Skewness
all	26.17	6.84	-0.04
high	19.1	3.13	9.23
low	35.15	1.65	2.03
up	28.63	5.06	-16.57
down	26.9	5.28	-14.7

2.3 Impact of Space Weather Events

In order to get a closer view on the impact of the space weather in the propagation time, three different space weather events from 2003 peak cycle have been selected for analysis.

- Halloween 2003: this event is a strong storm, with two peaks, so it looks like a twin storm even if it is considered to be a single storm.
- November 2003: this event presents a moderate storm.
- Enhanced March 2003: this event is not a single event but rather an extended period of time with activity higher than usual.

Figure 12 shows the re-entry time for the Halloween event. The *x*-axis is the bias time in days for the placement of the storm. A zero bias means that the storm begins at the beginning of the propagation. Positive bias means that the storm begins later during the propagation, for example, a bias of 10 days means that the storm starts ten days after the propagation has started, closer to the re-entry time. A bias of -10 days means that the storm starts ten days before the propagation starts, so it does not affect the propagation. However, not only the storm but all background activity is biased, there is some impact on the propagation even if the storm happens before or after the propagation period.

The largest impact on the propagation time (reducing it to 20 days) happens when the storm starts at the beginning of the propagation. As the time bias is increased (the storm starts later), the impact is lower and lower. At 25 days the storm no longer affects the propagation, as it happens 25 days after the 25-days re-entry period. There is another valley at time bias about -22 days. That corresponds to the November storm and is shown centred in Figure 13.

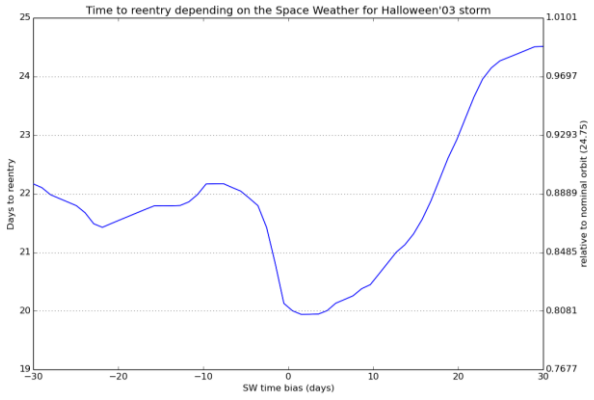

Figure 12: Time to re-entry for Halloween'03 storm

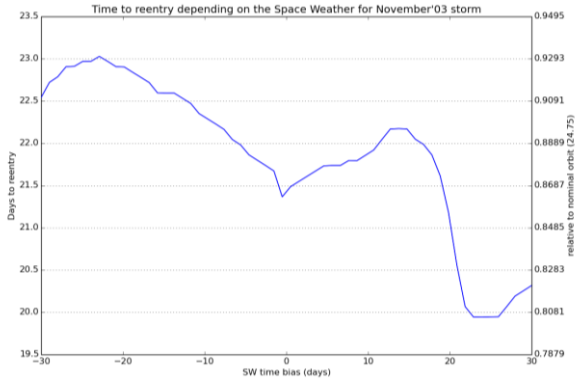

Figure 13: Time to re-entry for November'03 storm

The same analysis done for the enhanced period of March 2003 is shown in Figure 14.

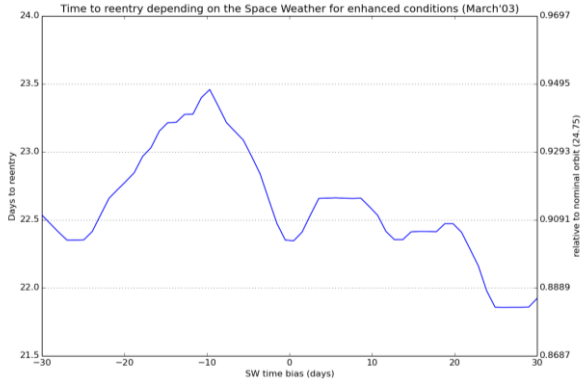

Figure 14: Time to re-entry for the enhanced activity period of March'03

2.4 Impact of the Predicted and Observed Solar Activity

In order to evaluate the impact of the solar activity forecast uncertainty, an analysis of the re-entry time

estimation is done considering the observed solar activity parameters, and the forecasted ones along the re-entry period.

The data used for this analysis is based on NOAA forecasts (provided by Dr Vallado) and those computed by ESA, provided by ESOC/Space Debris Office. Daily forecasts along October-November 2013 are used. These forecast files include the solar and geomagnetic parameters for the subsequent days, so they can be used for propagation of the GOCE orbit.

The simulation cases are prepared, considering the orbit propagation in the basis of observed space weather proxies up to the running day, and forecasted values up to the re-entry time. As an example, a simulation case tagged at 25/10/2013 considers observed data from 21/10/2016 (starting point for propagation in all cases) up to 25/10/2013 and forecasted data onwards (until re-entry time). The propagations are compared with the nominal propagation case, based on observed proxies.

The forecasts considered for this analysis on the geomagnetic, and solar data are summarised in the following figures. Figures provide the forecasted values for all simulated cases, where we can observe the large variability of estimated parameters when compared with the observed data.

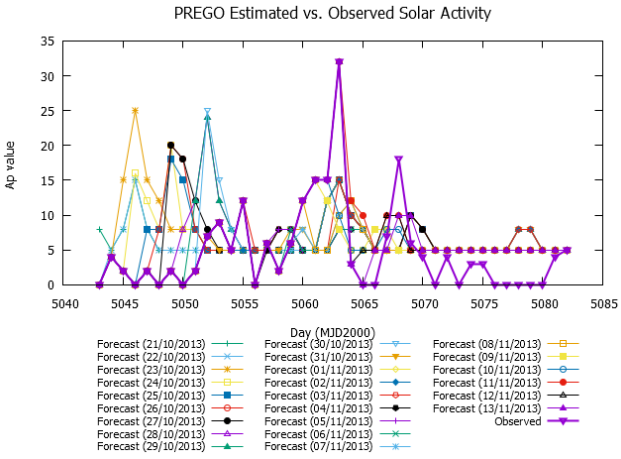

Figure 15: NOAA Forecast for Ap value along the analysed period

Considering these input values for the simulations, the obtained re-entry prediction time is provided in plots within Figure 19. Figures are given in absolute value and as a ratio of the nominal 24.7 time for the case when the observed data is considered for propagation.

It can be observed that, for the two forecast cases, there is about a 5% variation of the re-entry predicted time. This variability is similar to that caused by having an uncertainty in the position knowledge of about 0.1 km.

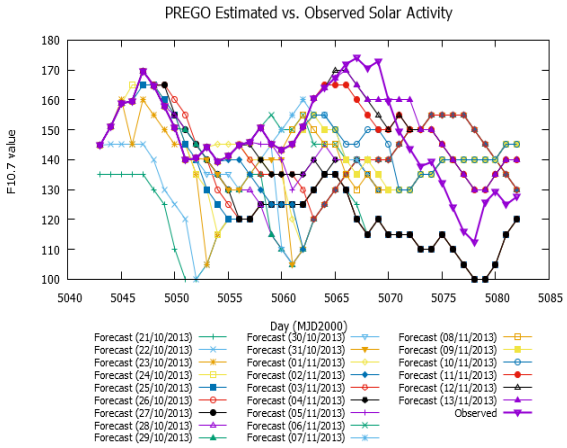

Figure 16: NOAA Forecast for F10.7 value along the analysed period

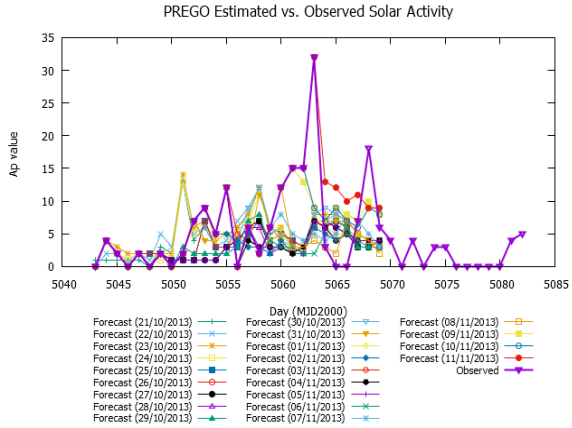

Figure 17: ESA Forecast for Ap value along the analysed period

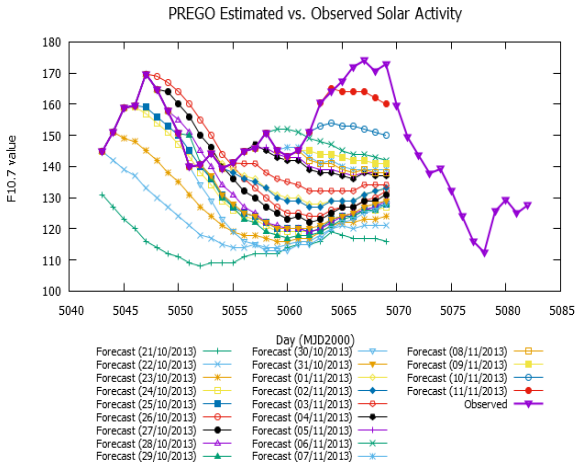

Figure 18: ESA Forecast for F10.7 value along the analysed period

The variations in the re-entry prediction are unpredictable as the forecast seems associated with large errors. This particular GOCE case analysed so far, occurred during a calm period, where forecast used to be better than in high solar activity periods, and thus, they can be considered optimistic for extracting general conclusions on other re-entry analysis.

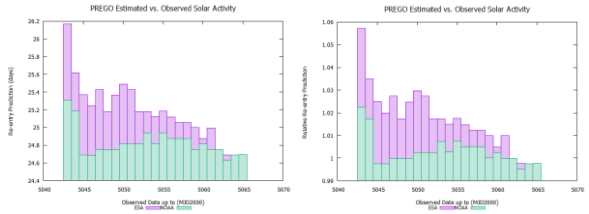

Figure 19: Comparison of Re-entry prediction evolution for the NOAA and ESA forecasted data used for propagation

In regards to the comparison of the two forecast systems, it has to be considered that the baseline data used for forecasting is the same (NOAA provided), and the forecast systems are then linked. Anyhow, the results are slightly different depending on the forecasting method.

Next figures provide some examples of the Ap and F10.7 values as estimated by the two forecast systems for a particular day, where differences among them are visible, although there is a similar agreement with the final observed data.

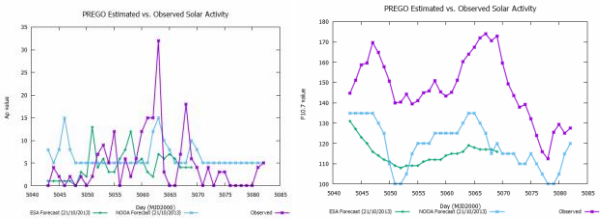

Figure 20: Comparison of the Observed Ap (left) and F10.7 (right) and the forecasted values by ESA and NOAA systems for the whole re-entry period

3 OBSERVATION MODEL ANALYSIS

Apart from the dynamic considerations reported above, an observational modelling has been undertaken. In this activity, two different aspects are covered: analysis of real observations of GOCE from TIRA radar, and an evaluation of different simulated observational approaches. Concerning *simulated observations*, different configurations in terms of number/location of sensors, observation accuracy and track length are analysed. This analysis allows feeding the dynamical sensitivity analysis with realistic predicted orbital information.

The simulated cases have been run with the AS4 simulator [3]. In order to validate the simulation results, a first comparison between the simulated measurements and the real ones was undertaken.

Twelve GOCE's tracks were observed from TIRA sensor during the re-entry phase in October-November 2013. These tracks have a duration between 6 or 5 minutes and covering a period of time about 20 days but with several gaps between them, for example between 6th and 7th tracks, there are 7 days without measurements.

The simulated observations are done over the precise orbit generated in the first task of the project, The comparison obtained, are quite acceptable. They fit properly and then, the use of simulated measurements for the sensor architecture analysis is realistic. Some differences can be associated the influence of the drag coefficient, which is more important when the object decays, and this value is changing with time in a real environment but in AS4 simulator is assumed as constant during all the execution.

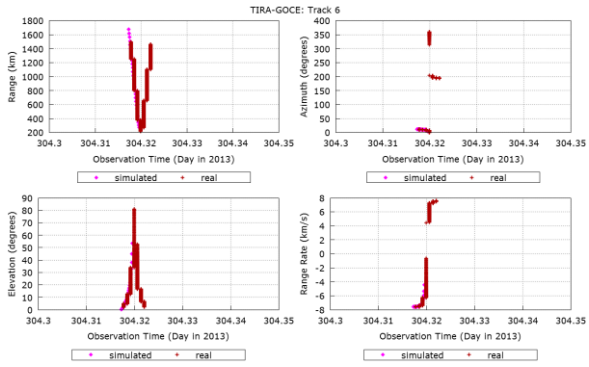

Figure 21: Comparison between real and estimated measurements for GOCE track 6 using precise orbit

3.1 Analysed Sensors Architectures

Different architectures of sensors have been analysed, all of them considering, that two tracks of the objects are processed together (one ascending in elevation and other one descending). A previous analysis was done in order to determine that this approach provides benefits in terms of orbital accuracy when compared with other approaches with single or multiple tracks processes together.

The main part of this activity is the execution of a sensitivity analysis focusing on different observation availability, sensor accuracies and data frequency. This sensitivity analysis is executed several observational approaches over a reference orbit, the OD on the basis

of those observational data, and the re-entry prediction at every orbital update. The predicted re-entry time is evaluated against the reference re-entry time in order to show the impact of the observational case onto the re-entry prediction capability.

The case of a unique sensor is compared with the case of having additional radar stations. These sensors are evenly distributed in Earth longitude, allowing a more continuous observation capacity. The number of sensors have an impact on the observational gap duration. The mean duration of gaps for only TIRA radar is 6 hours. When a second radar is considered this observation gap reduces down to 3 hours. Considering a third station the gap is reduced to 2 hours. With more than one site, there are large opportunities to observe the object and then the gap is reduced.

Figure 22 shows the OD errors for these architectures. Plots in first column are the real position and velocity errors (the difference between the real simulated orbit and the estimated one) and the second column shows the predicted errors by the covariance matrix. The lines are an average for each Orbit determination filter iteration (red is for one radar, green shows the errors using two radars and finally blue colour is for three radars). The main difference comes from adding additional sites and it is not encountered a significant improvement in the orbit accuracy with the length of tracks (also analysed as independent parameter).

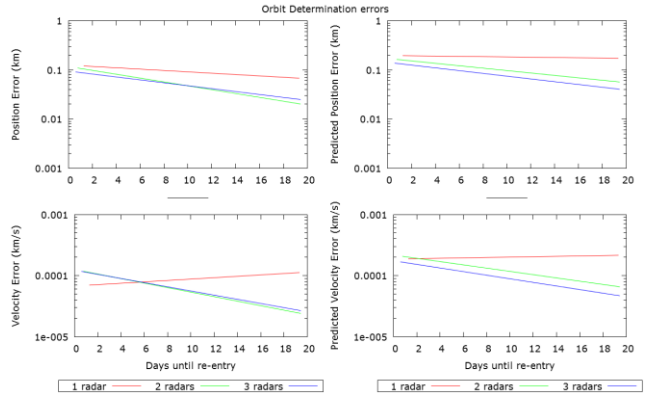

Figure 22: Orbit determination errors, comparison between 1, 2 or 3 radars evenly distributed in longitude. First column shows the real errors and second column are the errors predicted by covariance matrix

The OD errors for each architecture can be seen in following pictures with more detail. The upper plot shows the OD errors in position and velocity. In these pictures, red points are the real errors and green points are the error estimated by the covariance matrix. A fitting of these errors is represented by the lines blue and pink respectively (these lines are the same than Figure 22). Plots in the bottoms show the measurements (range, elevation, azimuth and Doppler) residuals during the OD.

The orbit accuracy improves with more than one sensor, but in these cases, there are two divergences as it can be seen with the light blue lines or in the measurements errors plots there is a peak in range residuals.

Similarly to the study with more than one radar evenly distributed in longitude, some tests have been executed using more than one radar station spaced in latitude (see Figure 24). Sensor 1 has similar characteristics and configuration than TIRA radar and the difference with the Sensor 2 is that this last one is located at -50º latitude. There are no appreciable differences in real position error.

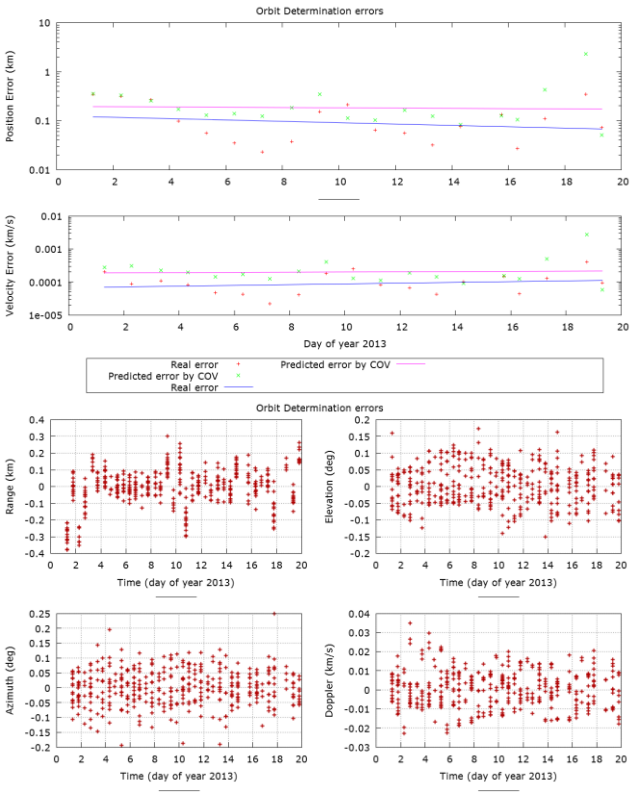

Figure 23: Orbit determination errors with 1 sensor and processing ascending-descending tracks. Upper plot shows the position and velocity errors and bottom plots are the residuals in measurements

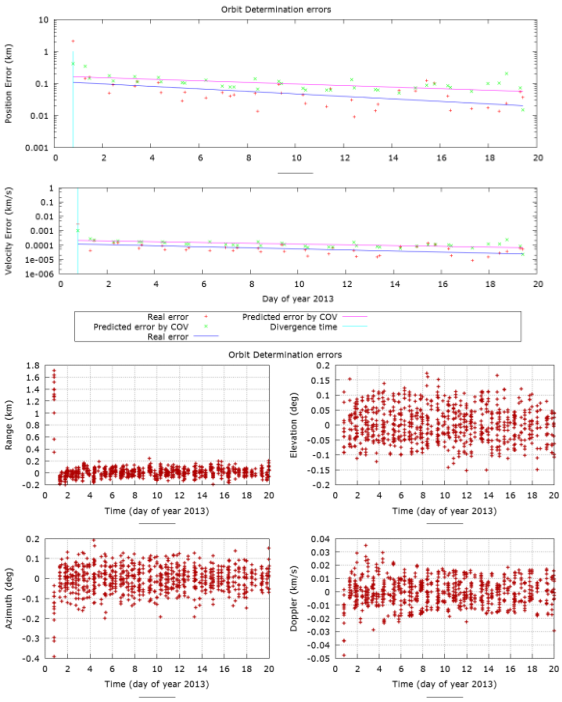

Figure 24: Orbit determination errors with 2 sensors (distributed in latitude) and processing ascending-descending tracks. Upper plots shows the position and velocity errors and bottom plots are the residuals in measurements

In regards to the re-entry prediction for the different configurations, AS4 Re-entry module is focused on the generation of the report of decaying objects. It provides re-entry reports with the objects decaying in the analysis period, including the best prediction of entry epoch and entry location. The reports are generated by medium-term numerical propagation of the catalogue.

This analysis relies on the comparison between the real and estimated re-entry dates using a set of estimated catalogues: three different estimated catalogues obtained by means of the generated measurements with 1, 2 or 3 sensors evenly distributed in longitude. The predicted orbit is computed 48 hours before to re-entry time (after processing the observations generated in each scenario).

Figure 25 illustrates the report associated to the estimated catalogues used in this analysis. Re-entry report contains the predicted entry epoch and location for the object. Together with the estimated data, the real re-entry is also reported, and the error in the estimation (time and position) is provided in the last column. It can be seen how the position re-entry error decreases with the number of sensors and the time re-entry error is minimal, only a few seconds for all cases. Moreover, with only 1 sensor the results are very acceptable.

SPACE SURVEILLANCE SYSTEM SYMULATOR RE-ENTRY ANALYSIS REPORT

			ESTIMATED REENTRY			REAL WORLD REENTRY			ERROR	
CODE	SATNAME	ENTRY EPOCH	LONG	LAT	ENTRY EPOCH	LONG	LAT	TIME(H)	POS(KM)	
1 SENSOR	34602	2013:11:11	0:15:25.9	-62.01	-49.12	2013:11:11	0:15:03.4	-61.50	-50.64	0.0062	174.5557
2 SENSORS	34602	2013:11:11	0:14:48.0	-61.13	-51.68	2013:11:11	0:15:03.4	-61.50	-50.64	0.0043	120.3433
3 SENSORS	34602	2013:11:11	0:14:55.2	-61.30	-51.19	2013:11:11	0:15:03.4	-61.50	-50.64	0.0023	64.2222

Figure 25: Re-entry report with 3 sensors and processing ascending-descending tracks

The following picture shows GOCE re-entry position in longitude and latitude. Blue point is the real re-entry (-60º,-56º) near to Falkland Island. Light blue is the re-entry computed by AS4 propagator and it is the considered value as real in our simulations. Then, red, green and violet are the estimated re-entry position during the orbit computation using one, two or three sites.

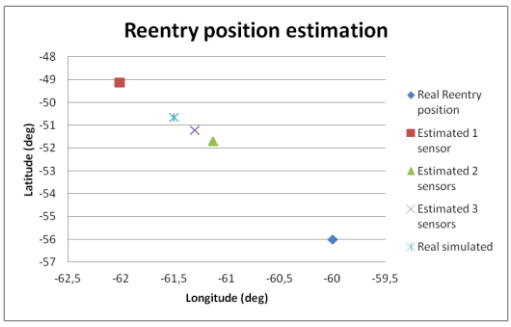

Figure 26: Re-entry position estimation where red point is real re-entry position and the other points indicate the positions given by AS4 re-entry tool

3.2 Accuracy of Sensor Data

The TIRA sensor configuration is assumed as the baseline sensor with a typical measurement accuracy are 50m for range, 10m/s for Doppler and 0.06 degrees for azimuth and elevation angles.

In this section, a brief analysis using different accuracy for the sensor data has been done. Case labelled Accuracy 1 is the baseline, Accuracy 2 corresponds to more precise data (10 m, 10 m/s and 0.04 deg), and finally Accuracy 3 is for bad measurements (100 m, 50 m/s and 0.08 deg), .

A similar picture to Figure 22, where were compared the OD errors using a different number of sensors, is shown below with the comparison of the real and estimated errors for the three accuracy cases and using measurements from a radar similar to TIRA.

Accuracy 1 and 2 do not show many differences, but Accuracy 3 (worse accuracy of sensor data) provides a divergence at the beginning of the simulation and it is more unstable (real error is bigger than estimated by a covariance matrix, see blue line). The accuracy of TIRA

radar seems to be enough for re-entry computation and no relevant improvement is obtained when it is increased to lower sensor error values.

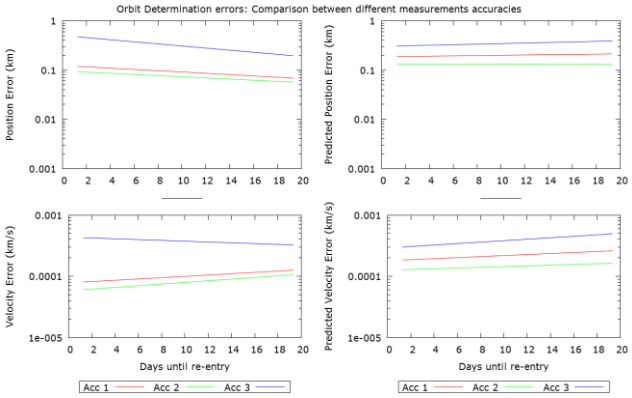

Figure 27: Comparison of Orbit determination errors with different measurements accuracy and 1 sensor

Similar analysis using these three accuracy levels have been executed with the architectures in former section to complete the study.

There are two types of architectures; the first one with sensors distributed in longitude and the second one uses two sensors evenly distributed in latitude (TIRA sensor as a baseline). All these cases have been executed with different measurements accuracy and the results are reported in following pictures, for the case of longitude-distribution of sensors. Results look as expected; the improvement in accuracy would provide benefits in terms of orbit computation.

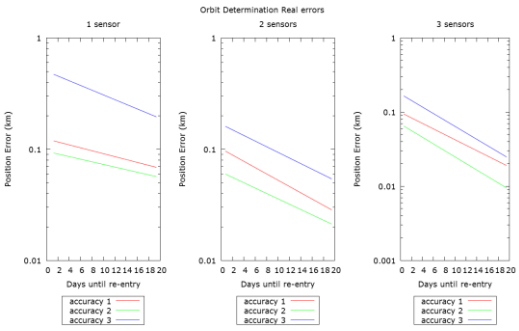

Figure 28: Comparison of orbit determination real errors with different measurements accuracy and different number of sensors (evenly distributed in longitude)

Finally, two pictures with the Along-track, Cross track and Radial errors along the orbital computation are included for all these cases (different number of sensors and different accuracy levels). At the beginning of the simulation, all cases show more instability and accuracy 3 presents the bigger errors especially when only one sensor is considered.

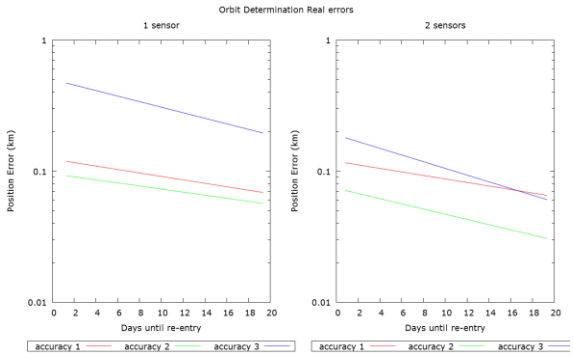

Figure 29: Comparison of orbit determination real errors with different measurements accuracy and different number of sensors (evenly distributed in latitude)

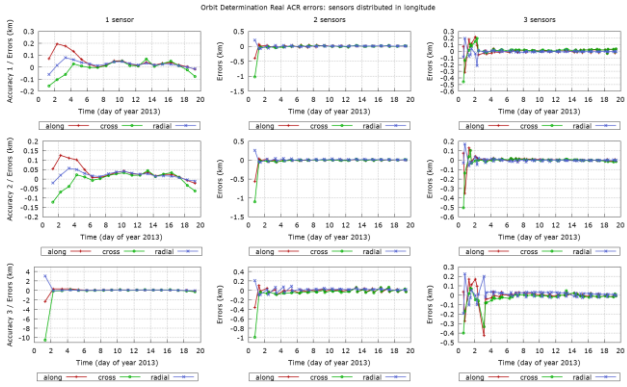

Figure 30: ACR errors for N sensors distributed in longitude and three accuracy levels

3.3 Impact of Observational Gap Periods

The duration of passes and the number of measurements inside a track improve the orbital results and achieve more accurate orbit, but they are not as important as the impact of the duration of gaps during the orbit computation, with the following profile:

- Case code 1 (Baseline), 20 days with measurements until re-entry time)
- Case code 2, only even days are processed (10 days with measurements)
- Case code 3, only odd days are processed (10 days with measurements)
- Case code, Two following days without measurements
- Case code 5Three following days without measurements
- Case code 6, Four following days without measurements

- Case code 7, Five following days without measurements
- Case code 8, Measurements at similar times than real tracks (with large gaps)

Figure 31 shows the OD position errors for all analysed cases. In these plots, red points are the real position errors (simulated and estimated orbit differences) and green points are the errors provided by the covariance matrix. Lines blue and pink are the average of these errors respectively. The light blue line indicates divergences during the orbit execution, in these cases, the real orbit with an error given by the covariance is assumed as estimated orbit for next orbit determination iteration.

In general, with measurements gaps, the distance between the real error and the one estimated by the covariance matrix increases for longer gap intervals as shown in the pictures, indicating the difficulties of the filter to properly estimate the orbit if very long gaps exist. Although this would not be a divergence, the estimated error is quite away from the real error. The cases where this does not happen are those who have had some divergence and the filter has been reset. The case gap_8 where the measurements are at similar times than real tracks, SRIF does work well because the estimated error is always more optimistic than the real one and even there are three divergence instances where the orbit is restored.

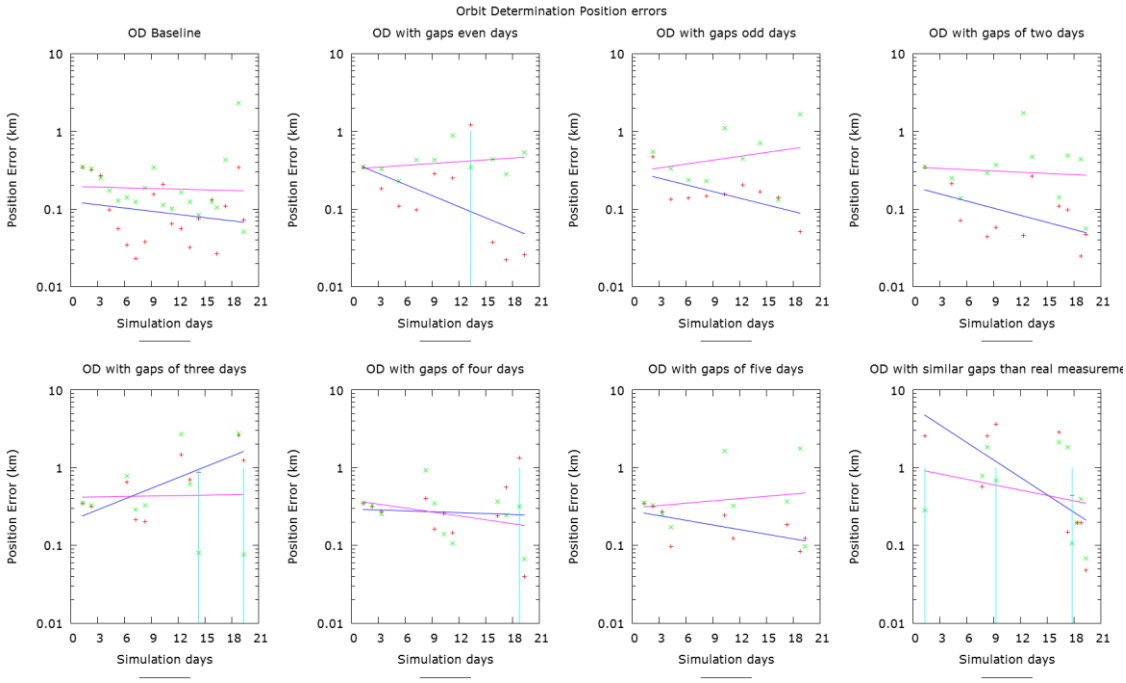

Figure 31: OD position errors for a set of gaps in measurements

SPACE SURVEILLANCE SYSTEM SYMULATOR RE-ENTRY ANALYSIS REPORT

		ESTIMATED REENTRY			REAL WORLD REENTRY			ERROR	
CODE	SATNAME	ENTRY EPOCH	LONG	LAT	ENTRY EPOCH	LONG	LAT	TIME(H)	POS(KM)
1	34602	2013:11:11 0:15:25.9	-62.01	-49.12	2013:11:11 0:15: 3.4	-61.50	-50.64	0.0062	174.5557
2	34602	2013:11:11 0:14:26.1	-60.57	-53.17	2013:11:11 0:15: 3.4	-61.50	-50.64	0.0104	291.6120
3	34602	2013:11:11 0:14:31.5	-60.71	-52.80	2013:11:11 0:15: 3.4	-61.50	-50.64	0.0089	249.2662
4	34602	2013:11:11 0:14:40.0	-60.93	-52.23	2013:11:11 0:15: 3.4	-61.50	-50.64	0.0065	182.9764
5	34602	2013:11:11 0:14:47.5	-61.11	-51.72	2013:11:11 0:15: 3.4	-61.50	-50.64	0.0044	124.6371
6	34602	2013:11:11 0:17:15.0	-64.20	-41.72	2013:11:11 0:15: 3.4	-61.50	-50.64	0.0366	1021.0601
7	34602	2013:11:11 0:15: 9.2	-61.63	-50.25	2013:11:11 0:15: 3.4	-61.50	-50.64	0.0016	44.7267
8	34602	2013:11:11 0:14:43.1	-61.01	-52.02	2013:11:11 0:15: 3.4	-61.50	-50.64	0.0056	158.6821

Figure 32: Re-entry report with different cases of gaps between tracks and processing ascending-descending tracks

Similar to the performed analysis in former section where the re-entry analysis is performed with more than one sensor, the re-entry prediction are analysed using a set of scenarios where the orbit was computed using measurements with different gaps between tracks.

Figure 32 illustrates a screenshot showing the report associated to the estimated catalogues used in this analysis. Re-entry report contains the predicted entry epoch and location for the object.

4 CONCLUSIONS

During the work reported in this paper related to the dynamic model analysis, several aspects affecting the dynamic of the re-entry prediction have been analysed.

First the uncertainty in position and velocity impact is investigated, concluding, through Monte Carlo analysis that, as expected, the size of the position and velocity uncertainty directly map to the re-entry prediction error. Velocity errors play a major role in the prediction error.

Consideration of spherical and elliptical covariance matrix does not seem to vary the behaviour. Typical uncertainties derived from radar observations can lead to up 10% of prediction error when propagating about 25 days.

Regarding the impact of space weather modelling, it can be highlighted that the lack of knowledge and predictability of the Space Weather conditions poses a strong influence on the re-entry predictions. Presence of storms is very relevant, although difficult to predict. Current forecast capability of Space Weather is very much limited, observing differences in the two analysed models. Of course, solar cycle impact is relevant, and shall be accounted for any re-entry prediction analysis

In regards to the observational model analysis, the paper shows different approaches for processing measurements for different sensor architectures, accuracy of the data and observational profile.

From the simulation analysis of different observational approaches, it seems that one sensor like TIRA allows predicting the orbit with good accuracy, although some benefits are shown if two observation sites are available. Regarding the accuracy, as expected, the better accuracy of the sensor error improves the results but it seems that TIRA's current accuracy is again enough for predictions.

The duration of tracks and the number of measurements inside a track does not seem as important as gaps between tracks (although they would improve the results). Large gaps between tracks (days) destabilise the filter (SRIF). The length of observing gaps between observing tracks plays a major role in the final achievable accuracy.

Re-entry analysis was performed with measurements from 1, 2 and 3 radars with good results for all of them. For the case of three sensors, the difference between the estimated re-entry and the real one is in the order of seconds and about 60 km in position (near to Falkland Island).

5 ACKNOWLEDGEMENTS

The work reported in this paper has been done in the frame of ESA PREGO contract (ESA/ESOC 4000115173/15/F/MOS).

The project has been undertaken by DEIMOS Space S.L.U, CNES and University of Bern.

6 REFERENCES

1. Technical Note on High Accuracy Orbit Determination (WP1000), PREGO-DMS-TNO-0001, 08/06/2016
2. C. Parigini, D. Bonetti, G. Blanco Arnao, N. Sanchez-Ortiz, S. Lemmens, Attitude Characterization of Aerodynamic Stable Objects Based on TLE, Proceedings of 7th European Conference on Space Debris, ESA/ESOC, 2017
3. N. Sánchez-Ortiz, E. Olmedo-Casal, N. Guijarro-López, M. Belló-Mora, AS4, A Simulator Supporting the Definition of the European Space Surveillance Segment of ESA, 1st European Space Surveillance Conference, Madrid 2011